

Anomalous high-magnetic field electronic state of the nematic superconductors $\text{FeSe}_{1-x}\text{S}_x$

M. Bristow,¹ P. Reiss,¹ A. A. Haghighirad,^{1,2} Z. Zajicek,¹ S. J. Singh,¹
T. Wolf,² D. Graf,³ W. Knafo,⁴ A. McCollam,⁵ and A. I. Coldea^{1,*}

¹*Clarendon Laboratory, Department of Physics, University of Oxford, Parks Road, Oxford OX1 3PU, UK*

²*Institut für Festkörperphysik, Karlsruhe Institute of Technology, 76021 Karlsruhe, Germany*

³*National High Magnetic Field Laboratory and Department of Physics,
Florida State University, Tallahassee, Florida 32306, USA*

⁴*Laboratoire National des Champs Magnétiques Intenses (LNCMI-EMFL),
UPR 3228, CNRS-UJF-UPS-INSA, 143 Avenue de Rangueil, 31400 Toulouse, France*

⁵*High Field Magnet Laboratory (HFML-EMFL), Radboud University, 6525 ED Nijmegen, The Netherlands*

(Dated: November 8, 2021)

Understanding superconductivity requires detailed knowledge of the normal electronic state from which it emerges. A nematic electronic state that breaks the rotational symmetry of the lattice can potentially promote unique scattering relevant for superconductivity. Here, we investigate the normal transport of superconducting $\text{FeSe}_{1-x}\text{S}_x$ across a nematic phase transition using high magnetic fields up to 69 T to establish the temperature and field-dependencies. We find that the nematic state is an anomalous non-Fermi liquid, dominated by a linear resistivity at low temperatures that can transform into a Fermi liquid, depending on the composition x and the impurity level. Near the nematic end point, we find an extended temperature regime with $\sim T^{1.5}$ resistivity. The transverse magnetoresistance inside the nematic phase has a $\sim H^{1.55}$ dependence over a large magnetic field range and it displays an unusual peak at low temperatures inside the nematic phase. Our study reveals anomalous transport inside the nematic phase, driven by the subtle interplay between the changes in the electronic structure of a multi-band system and the unusual scattering processes affected by large magnetic fields and disorder.

Magnetic field is a unique tuning parameter that can suppress superconductivity to reveal the normal low-temperature electronic behavior of many unconventional superconductors [1, 2]. High-magnetic fields can also induce new phases of matter, probe Fermi surfaces and determine the quasi-particle masses from quantum oscillations in the proximity of quantum critical points [1, 3]. In unconventional superconductors, close to antiferromagnetic critical regions, an unusual scaling between a linear resistivity in temperature and magnetic fields was found [4, 5]. Magnetic fields can also induce metal-to-insulator transitions, as in hole-doped cuprates, where superconductivity emerges from an exotic electronic ground state [2].

FeSe is a unique bulk superconductor with $T_c \sim 9$ K which displays a variety of complex and competing electronic phases [6]. FeSe is a bad metal at room temperature and it enters a nematic electronic state below $T_s \sim 87$ K. This nematic phase is characterized by multi-band shifts driven by orbital ordering that lead to Fermi surface distortions [6, 7]. Furthermore, the electronic ground state is that of a strongly correlated system and the quasiparticle masses display orbital-dependent enhancements [7, 8]. FeSe shows no long-range magnetic order at ambient pressure, but complex magnetic fluctuations are present at high energies over a large temperature range [9]. Below T_s , the spin-lattice relaxation rate from NMR experiments is enhanced as it captures the low-energy tail of the stripe spin-fluctuations [10, 11]. Furthermore, recent μSR studies invoke the close proximity of FeSe to a magnetic quantum critical point as the muon relaxation rate shows unusual temperature dependence inside the nematic state [12].

The changes in the electronic structure and magnetic fluctuations of FeSe can have profound implication on its transport and superconducting properties. STM reveals a highly

anisotropic superconducting gap driven by orbital-selective Cooper pairing [13]. Due to the presence of the small inner bands, whose Fermi energies are comparable to the superconducting gap, FeSe was placed inside the BCS-BEC crossover regime [14]. In large magnetic fields, when the Zeeman energy is comparable to the gap and Fermi energies, a peculiar highly-polarized superconducting state may occur [14].

To establish the role played by different competing interactions on nematicity and superconductivity, an ideal route is provided by the isoelectronic substitution of selenium by sulphur ions in $\text{FeSe}_{1-x}\text{S}_x$ [15]. This tuning parameter suppresses nematicity and it leads to changes in the electronic structure, similar to the temperature effects, with the Fermi surface becoming isotropic in the tetragonal phase and the electronic correlations becoming weaker [3, 6, 15, 16]. As nematicity is suppressed, it creates ideal conditions to explore a potential nematic critical point [17] in the absence of magnetism. The superconducting dome extends outside the nematic state but anisotropic pairing remains robust [18] and a different superconducting state was suggested to be stabilized in the tetragonal phase [19].

In this paper we study the normal electronic state across the nematic transition in $\text{FeSe}_{1-x}\text{S}_x$ using magnetotransport studies in high-magnetic fields up to 69 T. We find that the nematic state has a non-Fermi-liquid behaviour with an unusual transverse magnetoresistance ($\sim H^{1.55}$), reflecting an unconventional scattering mechanism. Just outside the nematic phase, resistivity is dominated by a $\sim T^{1.5}$ dependence, similar to studies under pressure [20]. The transverse magnetoresistance is significant inside the nematic phase and it shows an unusual change in slope at low temperatures. Inside the nematic phase at low temperatures, we find linear resistivity followed by Fermi-liquid behaviour for certain x and

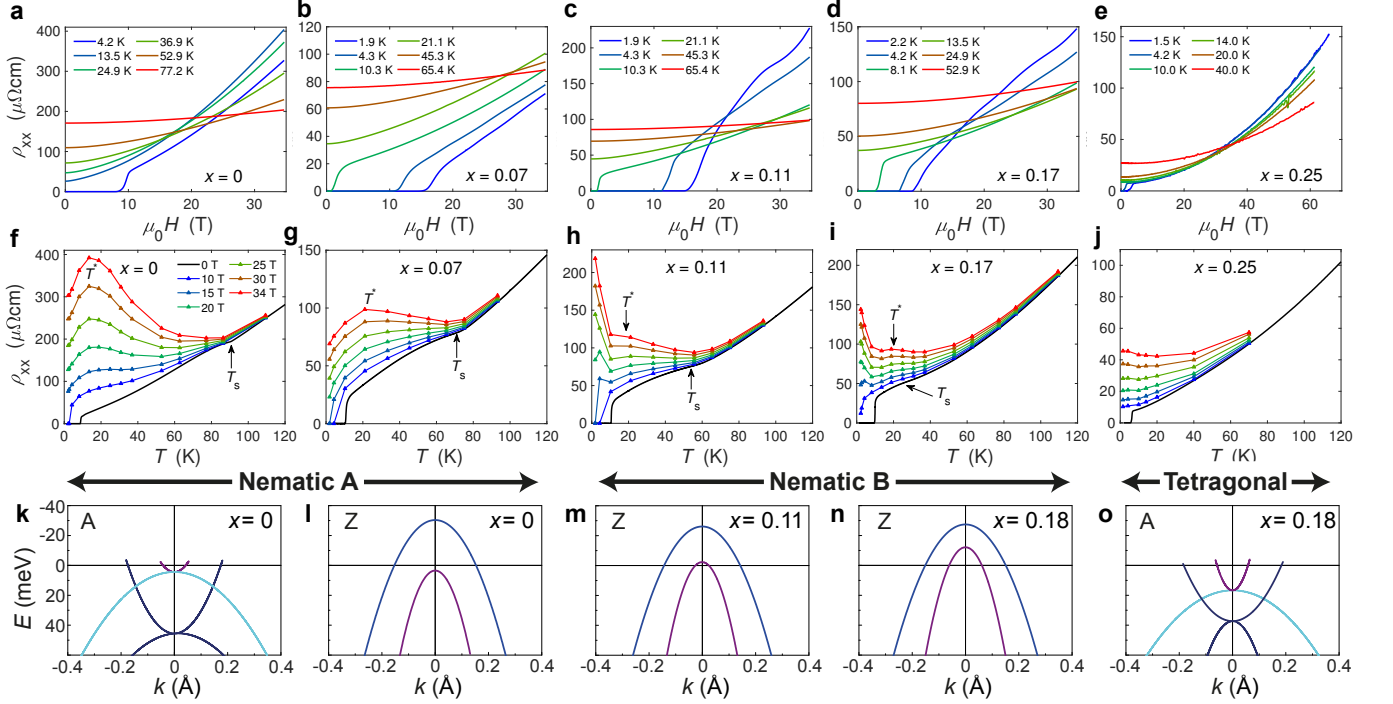


FIG. 1. **Transverse magnetoresistance of the nematic and tetragonal FeSe_{1-x}S_x.** (a-e) Field-dependent in-plane resistivity at different constant temperatures for different compositions, x , inside and outside the nematic phase. The magnetic field is applied along the c -axis, perpendicular to the in-plane electrical current. A strong magnetoresistance develops inside the nematic phase. (f-j) Resistivity against temperature in zero field (solid line) and at fixed magnetic fields (symbols), as extracted from the top panel for different x . The peak in magnetoresistance is indicated by T^* and the nematic phase emerges at T_s . (k-o) Schematic band dispersion at low temperatures at two high symmetry points at the top of the Brillouin zone, Z and A for different x (based on ARPES data reported in Refs.6, 7, 15, and 16). The horizontal lines represent the location of distinct regions in the magnetotransport behaviour called nematic A ($x = 0, 0.07$), nematic B ($x = 0.11, 0.17$) and the tetragonal phase for $x \gtrsim 0.18$. In the tetragonal phase, the compensated semi-metal is formed of two electron and two-hole like bands. Deep inside the nematic phase the inner hole band and inner electron bands are brought in the vicinity of the Fermi level.

impurity levels. Our study reveals anomalous transport in the nematic state due to the subtle changes in the electronic structure and/or scattering, which are also influenced by impurity levels.

RESULTS AND DISCUSSION

Figs. 1a-e show the transverse magnetoresistance, ρ_{xx} , of different single crystals of Fe(Se_{1-x}S_x) up to 35 T at various fixed temperatures inside the nematic phase and up to 69 T for $x \sim 0.25$ in the tetragonal phase. From these constant temperature runs, we can extract the magnetoresistance at fixed fields for each composition x , as shown in Fig. 1f-j, which reveals several striking features. Firstly, the magnetoresistance increases significantly once a system enters the nematic state at T_s , and its magnitude depends on the concentration x , being largest for FeSe, just above T_c . Secondly, in the vicinity of T_c in magnetic fields much larger than the upper critical field, the magnetoresistance shows an unusual temperature dependence that varies strongly with x across the phase diagram, as shown in Fig. 1(f-g). The resistivity slope $d\rho_{xx}/dT$ in 34 T of FeSe changes sign around a crossover temperature, $T^* \sim 14$ K, as shown in Fig. 1f (also in the colour plot of the slope in Fig. 3d). With increasing sulphur substitution from FeSe towards $x \sim 0.07$ (defined as the nematic A region), the position

of T^* shifts to a slightly higher temperature of ~ 20 K, and the peak in magnetoresistance is much smaller than for FeSe. For higher concentrations, approaching the nematic phase boundary, ($x \sim 0.11 - 0.17$ defined as the nematic B region), there is a small peak at T^* but the negative slope $d\rho_{xx}/dT$ in 34 T is strongly enhanced at low temperatures, different from the nematic A phase (see Fig. 1(h,i) and Fig. 3(d)). Lastly, in the tetragonal phase, the magnetoresistance shows a conventional behaviour and increases quadratically in magnetic fields (Fig. 1(e) and (j)).

The unusual downturn in resistivity in high-field fields below T^* inside the nematic A phase was previously assigned to large superconducting fluctuations in FeSe in magnetic fields up to 16 T [10, 11]. We find that this behaviour remains robust in magnetic fields at least a factor of 2 higher than the upper critical field of ~ 16 T for $H||c$ [10]. Furthermore, it also manifests in $x \sim 0.07$ inside the nematic A phase but it disappears for higher $x \gtrsim 0.1$. As T_c and the upper critical field inside the nematic phase for different x remain close to that of FeSe [3, 21], the changes in the resistivity slope in high magnetic fields are likely driven by field-induced effects that influence scattering and/or the electronic structure.

The Hall coefficient, $R_H = \rho_{xy}/\mu_0 H$, extrapolated in the

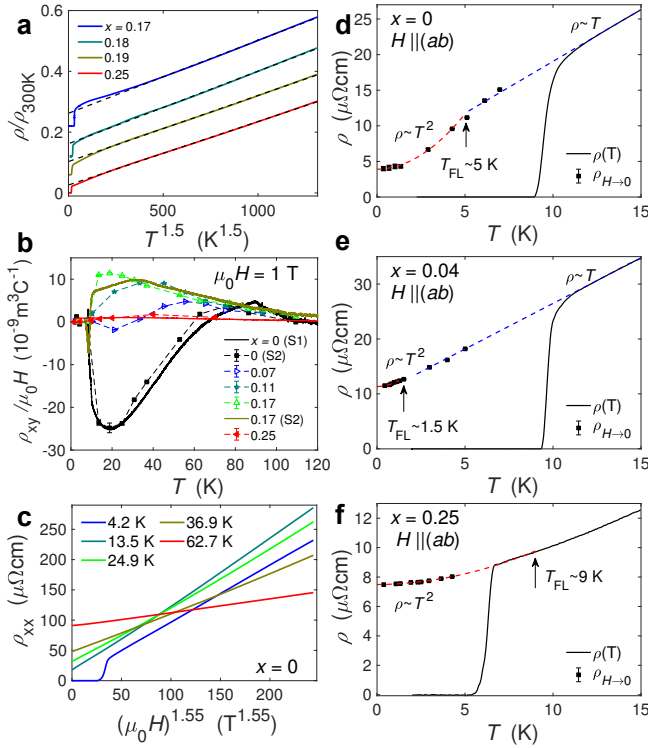


FIG. 2. **Normal electronic state of $\text{FeSe}_{1-x}\text{S}_x$.** (a) Temperature dependence of resistivity versus $T^{1.5}$ over a large temperature region just outside the nematic phase. (b) Hall effect coefficient in low magnetic fields, indicating the change in sign and the dominance of different highly mobile carriers across the nematic phase. (c) Resistivity versus $H^{1.55}$ for FeSe inside the nematic phase at constant temperatures. (d-f) The low-temperature linear resistivity. The solid lines are the zero-field resistivity data. Solid circles represent the zero-field extrapolated values of ρ_{xx} when $H \parallel (ab)$ plane. The dashed lines represent fits to a Fermi-liquid behaviour found below T_{FL} , as indicated by arrows.

low-field limit (below 1 T) for $\text{FeSe}_{1-x}\text{S}_x$ has an unusual temperature dependence, as shown in Fig. 2b. For a compensated metal, the sign of the Hall coefficient depends on the difference between the hole and electron mobilities [22]. In the tetragonal phase above T_s and for $x \gtrsim 0.18$, R_H is close to zero (Fig. 2b), as expected for a two-band compensated metal. On the other hand, in the low-temperature nematic A phase the sign of R_H is negative suggesting that transport is dominated by a highly mobile electron band [15, 23]. It becomes positive inside the nematic B phase, dominated by a hole-like band (Fig. 2(a)). It is worth mentioning that inside the nematic B phase the quantum oscillations are dominated by a low-frequency pocket with light-mass that disappears at the nematic end point [3]. Thus, the behaviour of R_H is linked to the disappearance of a small 3D hole pocket center at the Z-point in FeSe below T_s and its re-emergence in the nematic B phase with x substitution around $x \sim 0.11$, as found in ARPES studies [15] and sketched in Fig. 1(m). Interestingly, the subtle changes in the electronic structure in $\text{FeSe}_{1-x}\text{S}_x$ seem to correlate with the different features observed both in

magnetoresistance (Fig. 1(f-i)) and in the Hall coefficient $|R_H|$ that shows a maximum near T^* (Fig. 2(b)). In a high magnetic field, the Hall component of FeSe is complex, changing sign and being non-linear [15, 21]. A magnetic field can induce changes in scattering and/or field-induced Fermi-surface effects in the limit when the cyclotron energy is close to the Zeeman energy. The smallest inner bands of $\text{FeSe}_{1-x}\text{S}_x$ shift in energy as a function of composition x (and temperature [3]), as shown in Figs. 1(k-o). Furthermore, Hall effect in iron-based superconductors can be affected by the spin fluctuations that induce mixing of the electron and hole currents [24].

Next, we attempt to quantify the magnetoresistance across the phase diagram and in the vicinity of the nematic end point in $\text{FeSe}_{1-x}\text{S}_x$, as shown in Fig. 1(a-e). At the lowest temperature, inside the nematic phase, the transverse magnetoresistance of most samples is dominated by quantum oscillations [3] making difficult to quantify its dependence. A near-linear magnetoresistance is detected for $x \sim 0.07$ in Fig. 1b and for a dirty sample (with low residual resistivity ratio ~ 8.5) in Fig. S9. The quasi-linear field magnetoresistance at low temperature can arise from squeezed trajectories of carriers in semiclassically large magnetic fields in case of small Fermi surfaces ($\omega_c \tau \gg 1$) [25, 26]. Another explanation for an almost linear magnetoresistance is the presence of mobility fluctuations caused by spatial inhomogeneities, as found in low carrier density systems [26–28].

Classical magnetoresistance in systems with a single dominant scattering time is expected to follow a H^2 dependence [25]. This results in Kohler’s rule, which is violated in $\text{FeSe}_{1-x}\text{S}_x$ suggesting that the magnetoresistance is not dominated by a single scattering time, as shown in Fig. S2(a-c). Magnetoresistance is quadratic in magnetic fields up to 69 T in the tetragonal phase ($x \geq 0.19$) (see Fig. 1e and Fig. S4(e-f)) but not inside the nematic phase. $\text{FeSe}_{1-x}\text{S}_x$ are compensated multi-band systems [6] where the high-field magnetoresistance is expected to be very large and dependent on scattering times of electron and hole bands [22]. Magnetoresistance has a complex form and instead simpler scaling have been sought to reveal its importance, in particular in the vicinity of critical points [4, 5]. For example, in $\text{BaFe}_2(\text{As}_{1-x}\text{P}_x)$ for $x \sim 0.33$ at the antiferromagnetic critical point, a universal $H - T$ scaling was empirically found between the linear resistivity in temperature and magnetic field [4]. For $\text{FeSe}_{1-x}\text{S}_x$ near the nematic end point at $x \sim 0.17$ we find that a $H - T$ dependence collapses onto a single curve, as shown in Fig. S2(e). Despite this, the energy scaling of magnetoresistance used to describe the antiferromagnetic critical point in Ref. [4] is not obeyed in the vicinity of the nematic end point in $\text{FeSe}_{1-x}\text{S}_x$, as detailed in Fig. S2(g-i). This could be due to additional constraints to be included either to account for the nematoelastic coupling [29] and/or the effect of impurities. For example, a very dirty sample of $\text{FeSe}_{1-x}\text{S}_x$ close to $x_{nom} \sim 0.18$ was recently suggested to obey $H - T$ scaling [30].

For reasons described above, we propose a different approach to model the magnetoresistance data in the nematic state of $\text{FeSe}_{1-x}\text{S}_x$, using a power law in magnetic fields

given by $\rho_{xx}(H) = \rho_0(H) + bH^\delta$. Strikingly, we find that all the magnetoresistance data inside the nematic phase can be described by a unique exponent $\delta \sim 1.55(5)$ over a large field window, as shown by the colour plot in Fig.3(c) as well as in Figs.2(c) and S4(a-d). A detailed method of the extraction of δ and its stability over a large temperature and field window is shown in Fig.S3. Furthermore, this gives $\delta \sim 2$ for samples in the tetragonal phase (see Fig.3(c)). Inside the nematic phase, the Fermi surface of $\text{FeSe}_{1-x}\text{S}_x$ distorts anisotropically [6, 7] and an unusual type of scattering could become operational due to presence of hot and cold spots along certain directions [31].

In the absence of magnetic field the transport behaviour can also be described by a power law, $\rho(T) = \rho_0 + AT^\gamma$. Fig. 3a shows a colour plot of the exponent γ , which is close to unity at low temperatures inside the nematic phase and becomes sublinear close to the nematic phase boundary, indicating a significant deviation from Fermi-liquid behaviour (a value of $\gamma=1.1(2)$ was previously reported for FeSe [32]). Outside the nematic phase a $T^{1.5}$ dependence of resistivity describes the data well over a large temperature range up to 120 K (see Fig. 2(a) and Fig.3(a)), in agreement with previous studies of $\text{FeSe}_{1-x}\text{S}_x$ under pressure [20]. Using the high-magnetic field data below T_c , we extract the low-temperature resistivity in the absence of superconductivity, $\rho_{H \rightarrow 0}(T)$. Fig. 2(d-f) shows resistivity against temperature for different values of x , together with the extrapolated high-field points, using longitudinal magnetoresistance when $H \parallel (ab)$ plane, shown in Fig.S5. We also use transverse magnetoresistance data to extract the zero-field resistivity, using the established power law $H^{1.55}$, as shown in Fig. S7. From both measurements, we find strong evidence for a linear resistivity in the low temperature regime, below T^* , inside the nematic phase. Linear resistivity was also detected from the 35 T temperature dependence of the longitudinal magnetoresistance in Ref.[33], however, it was assumed to occur near the *nematic critical point* defined as $x_{nom} \sim 0.16$, which corresponds to $x \sim 0.13$ in our phase diagrams in Fig.3 and Fig.S1(b) (as the resistivity derivative in Ref.[33] show a $T_s \sim 51$ K). At low temperatures, we observe that Fermi-liquid behaviour recovers in the tetragonal phase (see also Refs. [33, 34]) and inside the nematic phase, below T_{FL} (see Figs. 2(d-f) and 3(b)). This is strongly dependent on composition and impurity level, even in the vicinity of the nematic end point (see Figs. S8 and S9). We find that T_{FL} is highest for the samples with the largest residual resistivity ratio (above ~ 16) (see Figs.S1(c) and S6). Theoretical models suggest that the temperature exponent, γ , in vicinity of critical points is highly dependent on the presence of *cold spots* on different Fermi surfaces, due to the symmetry of the nematic order parameter [31, 35]. On the other hand, near an antiferromagnetic critical point in the presence of spin fluctuations the impurity level also affects the temperature exponent [36]. Furthermore, the scale at which the crossover to Fermi liquid behavior occurs at T_{FL} in nematic critical systems could depend on the strength of the coupling to the lattice [29].

An overall representation of the resistivity slope

$d\rho_{xx}(34\text{ T})/dT$ in 34 T for $\text{FeSe}_{1-x}\text{S}_x$ as a function of temperature is shown in the phase diagram in Fig. 3d. The low-temperature manifestation of the nematic A and B phases is clearly different below T^* . In order to identify possible sources of scattering responsible for these changes, we consider the role of spin fluctuations. Recent NMR data found that anti-ferromagnetic spin fluctuations are present inside the nematic phase of $\text{FeSe}_{1-x}\text{S}_x$, being strongest around $x \sim 0.1$ [37]. In FeSe, spin fluctuations are rather anisotropic [37, 38] and strongly field-dependent below 15 K [11]. Interestingly, the spin-fluctuations relaxation rate is enhanced below T^* (Fig. 3(d)), suggesting a correlation between spin-dependent scattering, the high-field magnetoresistance and the low-temperature transport inside the nematic state. High-magnetic fields are expected to align magnetic spins and could affect the energy dispersion of low-energy spin excitations and spin-dependent scattering in magnetic fields. In FeSe, the spin-relaxation rate in different magnetic fields up to 19 T deviates at T^* [11] but it remains relatively constant in 19 T at the lowest temperatures. This may suggest the variation in magnetoresistance in high magnetic fields at low temperatures in $\text{FeSe}_{1-x}\text{S}_x$ is more sensitive to the changes in the electronic behaviour rather to the spin fluctuations across the nematic phase.

The low-temperature regime below T^* displays linear resistivity, which is a potential manifestation of scattering induced by critical spin-fluctuations in clean systems [36]. μSR studies place FeSe near an itinerant antiferromagnetic quantum critical point at very low temperatures [12] and spin-fluctuations are only found inside the nematic state [11, 37]. On the other hand, close to the nematic end point in $\text{FeSe}_{1-x}\text{S}_x$ we find that resistivity is not linear in temperature but is dominated by a $T^{1.5}$ dependence. This is contrast to the linear resistivity found near a antiferromagnetic critical point in $\text{BaFe}_2(\text{As}_{1-x}\text{P}_x)$ [32]. Theoretically, $\gamma = 3/2$ could describe the resistivity caused by strong antiferromagnetic critical fluctuations in the dirty limit [36, 39]. However, in $\text{FeSe}_{1-x}\text{S}_x$ the spin fluctuations are suppressed and a Lifshitz transition was detected at the nematic end point [3]. At a nematic critical point the divergent fluctuations for different Fermi surfaces could display unusual power laws in resistivity, as discussed in Refs. [31, 35, 40]. To assess the critical behaviour, it is worth emphasizing that the effective masses associated to the outer hole bands do not show any divergence close to the nematic end point $x \sim 0.18$ [3]. This agrees with the variation of the $A^{1/2}$ coefficient (see Fig. S11) and previous studies under pressure [20], suggesting the critical nematic fluctuations could be quenched by the coupling to the lattice along certain directions in $\text{FeSe}_{1-x}\text{S}_x$.

The striking difference in magnetotransport behaviour between the nematic and tetragonal phase in $\text{FeSe}_{1-x}\text{S}_x$ can have significant implications on what kind of superconductivity is stabilized inside and outside the nematic phase as different pairing channels may be dominant in different regions, as found experimentally [18, 19]. Linear resistivity found at low temperatures inside the nematic state is present in the region

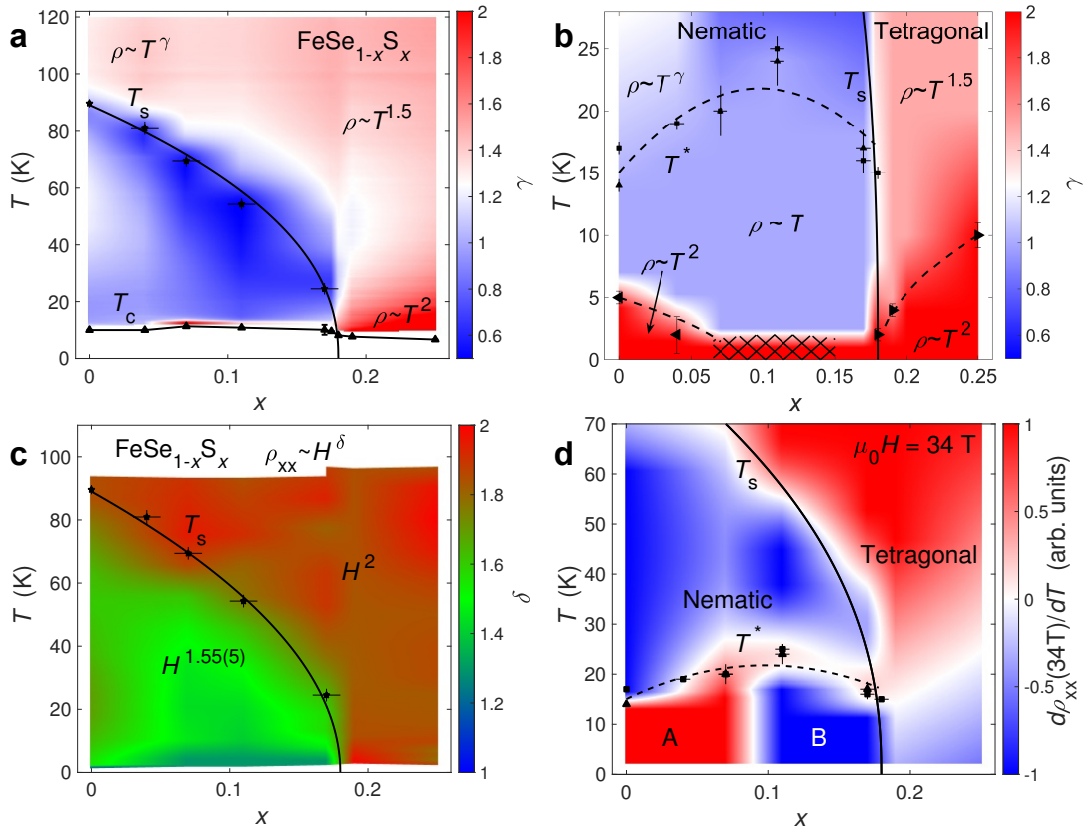


FIG. 3. **Phase diagrams of the resistivity exponents and high-field transport in FeSe_{1-x}S_x.** The colour plot of the temperature exponent, γ , extracted from (a) zero-resistivity data, as shown in Fig. S10. (b) The low-temperature resistivity exponent below T^* , extrapolated from high magnetic fields as shown in Figs. S5 and S7, indicating the non-Fermi liquid behaviour of the nematic phase. Fermi liquid recovers below T_{FL} for the compositions x with lowest disorder both inside the nematic phase and in the tetragonal phase. (c) The temperature dependence of field exponent δ showing a dominant $\sim H^{1.55}$ power law inside the nematic phase (based on Fig.S3). (d) The colour plot of the slope of resistivity in 34 T between the nematic A and B phases. Solid squares represent T_s and solid triangles T_c . T^* indicated by stars represents the peak in magnetoresistance and the maximum in $|R_H|$. Solid lines indicate the nematic and superconducting phase boundaries and the dashed lines are guides to the eye. The hashed region at low temperatures in (b) has not yet been accessed experimentally.

where spin-fluctuations are likely to be present. Furthermore, the absence of superconductivity enhancement at the nematic end point in FeSe_{1-x}S_x is supported by the lack of divergent critical fluctuations, found both with chemical pressure [3] and applied pressure [20]. It is expected that the coupling to the relevant lattice strain restricts criticality in nematic systems only to certain high symmetry directions [29, 41].

In conclusion, we have studied the evolution of the low-temperature magnetotransport behaviour in FeSe_{1-x}S_x in high-magnetic fields up to 69 T. We find that the nematic state has non-Fermi liquid behaviour and displays unconventional power laws in magnetic field, reflecting the dominant anomalous scattering inside the nematic phase. In high magnetic fields, well-above the upper critical fields, the transverse magnetoresistance shows a change in slope that reflects the changes in the spin-fluctuations and/or the electronic structure. In the low-temperature limit, high magnetic field suppresses superconductivity and it reveals an extended linear resistivity in temperature followed by a Fermi-liquid like dependence, highly dependent on the composition and impurity

level. Our study reveals the anomalous transport behaviour of the nematic state, strikingly different from the tetragonal phase, that influences how superconductivity is stabilized in different phases.

MATERIALS AND METHODS

Single crystals of FeSe_{1-x}S_x were grown by the KCl/AlCl₃ chemical vapor transport method [42]. The composition for samples from the same batch were checked using EDX as reported previously in Ref. [3]. Note that in Refs.[30, 33] the nominal, x_{nom} were can be at least 80% less than the real x (see also Ref. [3, 17, 37]). The structural transition at T_s also provides useful information about the expected x value, as shown in Fig.S1. More than 30 samples were screened for high magnetic field studies to test their physical properties. Residual resistivity ratio varies between 15-44, as shown in Fig.S1c. We observed the variation within the same batch due to the inhomogeneous distribution of sulfur with increasing x (see Figs.S1 and S8). We estimate that the nematic end point is located close to $x \sim 0.180(5)$ (see Figs.S1) and S11).

In-plane transport measurements ($I||ab$) were performed

in a variable temperature cryostat in dc fields up to 38 T at HFML, Nijmegen and up to 70 T at LNCMI, Toulouse with the magnetic field applied mainly along the c -axis (transverse magnetoresistance) but also in the (ab) conducting plane (longitudinal magnetoresistance) at constant temperatures. Low-field measurements were performed in a 16 T Quantum Design PPMS. The resistivity ρ_{xx} and Hall ρ_{xy} components were measured using a low-frequency five-probe technique and were separated by (anti)symmetrizing data measured in positive and negative magnetic fields. Good electrical contacts were achieved by In soldering along the long edge of the single crystals and electrical currents up to 3 mA were used to avoid heating. Magnetic fields along the c -axis suppress superconductivity in fields higher than 20 T for all x values [3].

ACKNOWLEDGMENTS

We thank Lara Befatto, Dmitrii Maslov, Rafael Fernandes, Erez Berg, Shigeru Kasahara, Steve Simon, Siddharth Parameswaran and Stephen Blundell for useful comments and discussions. We thank and acknowledge previous contributions from Matthew Watson, Mara Bruma, Samuel Blake, Abhinav Naga and Nathaniel Davies. This work was mainly supported by EPSRC (EP/L001772/1, EP/I004475/1, EP/I017836/1). A.A.H. acknowledges the financial support of the Oxford Quantum Materials Platform Grant (EP/M020517/1). A portion of this work was performed at the National High Magnetic Field Laboratory, which is supported by National Science Foundation Cooperative Agreement No. DMR-1157490 and the State of Florida. Part of this work was supported supported by HFML-RU/FOM and LNCMI-CNRS, members of the European Magnetic Field Laboratory (EMFL) and by EPSRC (UK) via its membership to the EMFL (grant no. EP/N01085X/1). Part of this work was supported by Programme Investissements d Avenir under the programme ANR-11-IDEX-0002-02, reference ANR-10-LABX-0037-NEXT We also acknowledge the Oxford Centre for Applied Superconductivity and the Oxford John Fell Fund. A.I.C. acknowledges an EPSRC Career Acceleration Fellowship (EP/I004475/1).

FOOTNOTES

To whom correspondence may be addressed: amalia.coldea@physics.ox.ac.uk

Author contributions: A.I.C. designed, planned and supervised the research. M.B., P.R., Z.Z. and A.I.C. performed experiments in Nijmegen with support from A.M.; P.R. and A.I.C. performed experiments in Tallahassee with support from D.G.; M.B., P.R., and A.I.C. performed experiments in Toulouse with support from W.K.; A.A.H., T.W. and S.S. grew single crystals. M.B. and A.I.C. performed data analysis. A.I.C. and M.B. wrote the paper with contributions and comments from all the authors.

* corresponding author: amalia.coldea@physics.ox.ac.uk

- [1] B. J. Ramshaw, S. E. Sebastian, R. D. McDonald, James Day, B. S. Tan, Z. Zhu, J. B. Betts, Ruixing Liang, D. A. Bonn, W. N. Hardy, and N. Harrison, "Quasiparticle mass enhancement approaching optimal doping in a high- T_c superconductor," *Science* **348**, 317–320 (2015), <http://science.sciencemag.org/content/348/6232/317.full.pdf>.
- [2] G. S. Boebinger, Yoichi Ando, A. Passner, T. Kimura, M. Okuya, J. Shimoyama, K. Kishio, K. Tamasaku, N. Ichikawa, and S. Uchida, "Insulator-to-Metal Crossover in the Normal State of $\text{La}_{2-x}\text{Sr}_x\text{CuO}_4$ Near Optimum Doping," *Phys. Rev. Lett.* **77**, 5417–5420 (1996).
- [3] A. I. Coldea, S. F. Blake, S. Kasahara, A. A. Haghighirad, M. D. Watson, W. Knafo, E. S. Choi, A. McCollam, P. Reiss, T. Yamashita, M. Bruma, S. Speller, Y. Matsuda, T. Wolf, T. Shibauchi, and A. J. Schofield, "Evolution of the low-temperature Fermi surface of superconducting $\text{FeSe}_{1-x}\text{S}_x$ across a nematic phase transition," *npj Quantum Materials* **4**, 2 (2019).
- [4] Ian M. Hayes, Ross D. McDonald, Nicholas P. Breznay, Toni Helm, Philip J. W. Moll, Mark Wartenbe, Arkady Shekhter, and James G. Analytis, "Scaling between magnetic field and temperature in the high-temperature superconductor $\text{BaFe}_2(\text{As}_{1-x}\text{P}_x)_2$," *Nature Physics* **12**, 916 (2016).
- [5] P. Giraldo-Gallo, J. A. Galvis, Z. Stegen, K. A. Modic, F. F. Balakirev, J. B. Betts, X. Lian, C. Moir, S. C. Riggs, J. Wu, A. T. Bollinger, X. He, I. Božović, B. J. Ramshaw, R. D. McDonald, G. S. Boebinger, and A. Shekhter, "Scale-invariant magnetoresistance in a cuprate superconductor," *Science* **361**, 479–481 (2018).
- [6] A. I. Coldea and M. D. Watson, "The key ingredients of the electronic structure of FeSe," *Annu. Rev. Cond. Matt. Phys.* **9** (2018), 10.1146/annurev-conmatphys-033117-054137.
- [7] M. D. Watson, T. K. Kim, A. A. Haghighirad, N. R. Davies, A. McCollam, A. Narayanan, S. F. Blake, Y. L. Chen, S. Ghanadzadeh, A. J. Schofield, M. Hoesch, C. Meingast, T. Wolf, and A. I. Coldea, "Emergence of the nematic electronic state in FeSe," *Phys. Rev. B* **91**, 155106 (2015).
- [8] Matthew D. Watson, Steffen Backes, Amir A. Haghighirad, Moritz Hoesch, Timur K. Kim, Amalia I. Coldea, and Roser Valentí, "Formation of Hubbard-like bands as a fingerprint of strong electron-electron interactions in FeSe," *Phys. Rev. B* **95**, 081106 (2017).
- [9] Q. Wang, Y. Shen, B. Pan, X. Zhang, K. Ikeuchi, K. Iida, A. D. Christianson, H. C. Walker, D. T. Adroja, M. Abdel-Hafiez, X. Chen, D. A. Chareev, A. N. Vasiliev, and J. Zhao, "Magnetic ground state of FeSe," *Nat. Commun.* **7**, 12182 (2016).
- [10] S. Kasahara, T. Yamashita, A. Shi, R. Kobayashi, Y. Shimoyama, T. Watashige, K. Ishida, T. Terashima, T. Wolf, F. Hardy, C. Meingast, H. v. Löhneysen, A. Levchenko, T. Shibauchi, and Y. Matsuda, "Giant superconducting fluctuations in the compensated semimetal FeSe at the BCS-BEC crossover," *Nat. Commun.* **7**, 12843 (2016).
- [11] Anlu Shi, Takeshi Arai, Shunsaku Kitagawa, Takayoshi Yamanaka, Kenji Ishida, Anna E. Böhrer, Christoph Meingast, Thomas Wolf, Michihiro Hirata, and Takahiko Sasaki, "Pseudogap Behavior of the Nuclear Spin Lattice Relaxation Rate in FeSe Probed by ^{77}Se -NMR," *Journal of the Physical Society of Japan* **87**, 013704 (2018), <https://doi.org/10.7566/JPSJ.87.013704>.
- [12] V. Grinenko, R. Sarkar, P. Materne, S. Kamusella, A. Ya-

- mamshita, Y. Takano, Y. Sun, T. Tamegai, D. V. Efremov, S.-L. Drechsler, J.-C. Orain, T. Goko, R. Scheuermann, H. Luetkens, and H.-H. Klauss, “Low-temperature breakdown of antiferromagnetic quantum critical behavior in FeSe,” *Phys. Rev. B* **97**, 201102 (2018).
- [13] P. O. Sprau, A. Kostin, A. Kreisel, A. E. Böhmer, V. Taufour, P. C. Canfield, S. Mukherjee, P. J. Hirschfeld, B. M. Andersen, and J. C. Séamus Davis, “Discovery of Orbital-Selective Cooper Pairing in FeSe,” *Science* **357**, 75 (2016).
- [14] Shigeru Kasahara, Tatsuya Watashige, Tetsuo Hanaguri, Yuhki Kohsaka, Takuya Yamashita, Yusuke Shimoyama, Yuta Mizukami, Ryota Endo, Hiroaki Ikeda, Kazushi Aoyama, Taichi Terashima, Shinya Uji, Thomas Wolf, Hilbert von Löhneysen, Takasada Shibauchi, and Yuji Matsuda, “Field-induced superconducting phase of FeSe in the BCS-BEC crossover,” *Proc. Natl. Acad. Sci. U. S. A.* **111**, 16309 (2014).
- [15] M. D. Watson, T. K. Kim, A. A. Haghighirad, S. F. Blake, N. R. Davies, M. Hoesch, T. Wolf, and A. I. Coldea, “Suppression of orbital ordering by chemical pressure in FeSe_{1-x}S_x,” *Phys. Rev. B* **92**, 121108 (2015).
- [16] P. Reiss, M. D. Watson, T. K. Kim, A. A. Haghighirad, D. N. Woodruff, M. Bruma, S. J. Clarke, and A. I. Coldea, “Suppression of electronic correlations by chemical pressure from FeSe to FeS,” *Phys. Rev. B* **96**, 121103 (2017).
- [17] S. Hosoi, K. Matsuura, K. Ishida, Hao Wang, Y. Mizukami, T. Watashige, S. Kasahara, Y. Matsuda, and T. Shibauchi, “Nematic quantum critical point without magnetism in FeSe_{1-x}S_x superconductors,” *PNAS* **113**, 8139 (2016).
- [18] Yuki Sato, Shigeru Kasahara, Tomoya Taniguchi, Xiangzhuo Xing, Yuichi Kasahara, Yoshifumi Tokiwa, Youichi Yamakawa, Hiroshi Kontani, Takasada Shibauchi, and Yuji Matsuda, “Abrupt change of the superconducting gap structure at the nematic critical point in FeSe_{1-x}S_x,” *Proceedings of the National Academy of Sciences* (2018), 10.1073/pnas.1717331115.
- [19] T. Hanaguri, V. Iwaya, Y. Kohsaka, T. Machida, T. Watashige, S. Kasahara, T. Shibauchi, and Y. Matsuda, “Two distinct superconducting pairing states divided by the nematic end point in FeSe_{1-x}S_x,” *Sci. Adv.* **4**, eaar6419 (2018).
- [20] P. Reiss, D. Graf, A. A. Haghighirad, W. Knafo, L. Drigo, M. Bristow, A. J. Schofield, and A. I. Coldea, “Quenched nematic criticality separating two superconducting domes in an iron-based superconductor under pressure,” *arXiv:1902.11276* (2019).
- [21] M. Bristow, P. Reiss, A. A. Haghighirad, and A. I. Coldea, in preparation (2019).
- [22] M. D. Watson, T. Yamashita, S. Kasahara, W. Knafo, M. Nardone, J. Béard, F. Hardy, A. McCollam, A. Narayanan, S. F. Blake, T. Wolf, A. A. Haghighirad, C. Meingast, A. J. Schofield, H. v. Löhneysen, Y. Matsuda, A. I. Coldea, and T. Shibauchi, “Dichotomy between the Hole and Electron Behavior in Multiband Superconductor FeSe Probed by Ultrahigh Magnetic Fields,” *Phys. Rev. Lett.* **115**, 027006 (2015).
- [23] Yue Sun, Sunseng Pyon, and Tsuyoshi Tamegai, “Electron carriers with possible Dirac-cone-like dispersion in FeSe_{1-x}S_x (x=0 and 0.14) single crystals triggered by structural transition,” *Phys. Rev. B* **93**, 104502 (2016).
- [24] L. Fanfarillo, E. Cappelluti, C. Castellani, and L. Benfatto, “Unconventional hall effect in pnictides from interband interactions,” *Phys. Rev. Lett.* **109**, 096402 (2012).
- [25] A.B. Pippard, *Magneto-resistance in Metals*, Cambridge Studies in Low Temperature Physics (Cambridge University Press, 1989).
- [26] Xu Du, Shan-Wen Tsai, Dmitrii L. Maslov, and Arthur F. Hebard, “Metal-insulator-like behavior in semimetallic bismuth and graphite,” *Phys. Rev. Lett.* **94**, 166601 (2005).
- [27] A. Narayanan, M. D. Watson, S. F. Blake, N. Bruyant, L. Drigo, Y. L. Chen, D. Prabhakaran, B. Yan, C. Felser, T. Kong, P. C. Canfield, and A. I. Coldea, “Linear Magnetoresistance Caused by Mobility Fluctuations in *n*-Doped Cd₃As₂,” *Phys. Rev. Lett.* **114**, 117201 (2015).
- [28] John Singleton, “A simple transport model for the temperature-dependent linear magnetoresistance of high-temperature superconductors,” *arXiv:1810.01998* (2018).
- [29] I. Paul and M. Garst, “Lattice Effects on Nematic Quantum Criticality in Metals,” *Physical Review Letters* **118**, 1–5 (2017).
- [30] S. Licciardello, N. Maksimovic, J. Ayres, J. Buhot, M. Culo, B. Bryant, S. Kasahara, Y. Matsuda, T. Shibauchi, V. Nagara-jan, J. G. Analytis, and N. E. Hussey, “Coexistence of orbital and quantum critical magnetoresistance in FeSe_{1-x}S_x,” *arXiv:1903.05679* (2019).
- [31] Xiaoyu Wang and Erez Berg, “Scattering mechanisms and electrical transport near an Ising nematic quantum critical point,” *arXiv:1902.04590* (2019).
- [32] S. Kasahara, T. Shibauchi, K. Hashimoto, K. Ikada, S. Tonegawa, R. Okazaki, H. Shishido, H. Ikeda, H. Takeya, K. Hirata, T. Terashima, and Y. Matsuda, “Evolution from non-Fermi-to Fermi-liquid transport via isovalent doping in BaFe₂(As_{1-x}P_x)₂ superconductors,” *Phys. Rev. B* **81**, 184519 (2010).
- [33] S. Licciardello, J. Buhot, J. Lu, J. Ayres, S. Kasahara, Y. Matsuda, T. Shibauchi, and N. E. Hussey, “Electrical resistivity across a nematic quantum critical point,” *Nature* (2019), 10.1038/s41586-019-0923-y.
- [34] Takahiro Urata, Yoichi Tanabe, Khuong Kim Huynh, Hidetoshi Oguro, Kazuo Watanabe, and Katsumi Tanigaki, “Non-Fermi liquid behavior of electrical resistivity close to the nematic critical point in Fe_{1-x}Co_xSe and FeSe_{1-y}S_y,” (2016), *arXiv:1608.01044*.
- [35] Dmitrii L. Maslov, Vladimir I. Yudson, and Andrey V. Chubukov, “Resistivity of a Non-Galilean-Invariant Fermi Liquid near Pomeranchuk Quantum Criticality,” *Phys. Rev. Lett.* **106**, 106403 (2011).
- [36] A. Rosch, “Interplay of disorder and spin fluctuations in the resistivity near a quantum critical point,” *Phys. Rev. Lett.* **82**, 4280–4283 (1999).
- [37] P. Wiecki, K. Rana, A. E. Böhmer, Y. Lee, S. L. Bud’ko, P. C. Canfield, and Y. Furukawa, “Persistent correlation between superconductivity and antiferromagnetic fluctuations near a nematic quantum critical point in FeSe_{1-x}S_x,” *Phys. Rev. B* **98**, 020507 (2018).
- [38] R. X. Cao, Jun Dong, Q. L. Wang, X. S. Ye, J. B. Zhang, Y. F. Xu, D. A. Chareev, A. N. Vasiliev, Bing Wu, Guoqing Wu, and X. H. Zeng, “Observation of orbital ordering and origin of nematic order in FeSe,” *arxiv.1810.09639* (2018).
- [39] T. Moriya, *Spin fluctuations in itinerant electron magnetism*, Springer series in solid-state sciences (Springer-Verlag, 1985).
- [40] Luca Dell’Anna and Walter Metzner, “Electrical resistivity near pomeranchuk instability in two dimensions,” *Phys. Rev. Lett.* **98**, 136402 (2007).
- [41] D. Labat and I. Paul, “Pairing instability near a lattice-influenced nematic quantum critical point,” *Phys. Rev. B* **96**, 195146 (2017).
- [42] A. E. Böhmer, F. Hardy, F. Eilers, D. Ernst, P. Adelman, P. Schweiss, T. Wolf, and C. Meingast, “Lack of coupling between superconductivity and orthorhombic distortion in stoichiometric single-crystalline FeSe,” *Phys. Rev. B* **87**, 180505 (2013).

Supplemental Materials for Anomalous high-magnetic field electronic state of the nematic superconductors $\text{Fe}(\text{Se}_{1-x}\text{S}_x)$

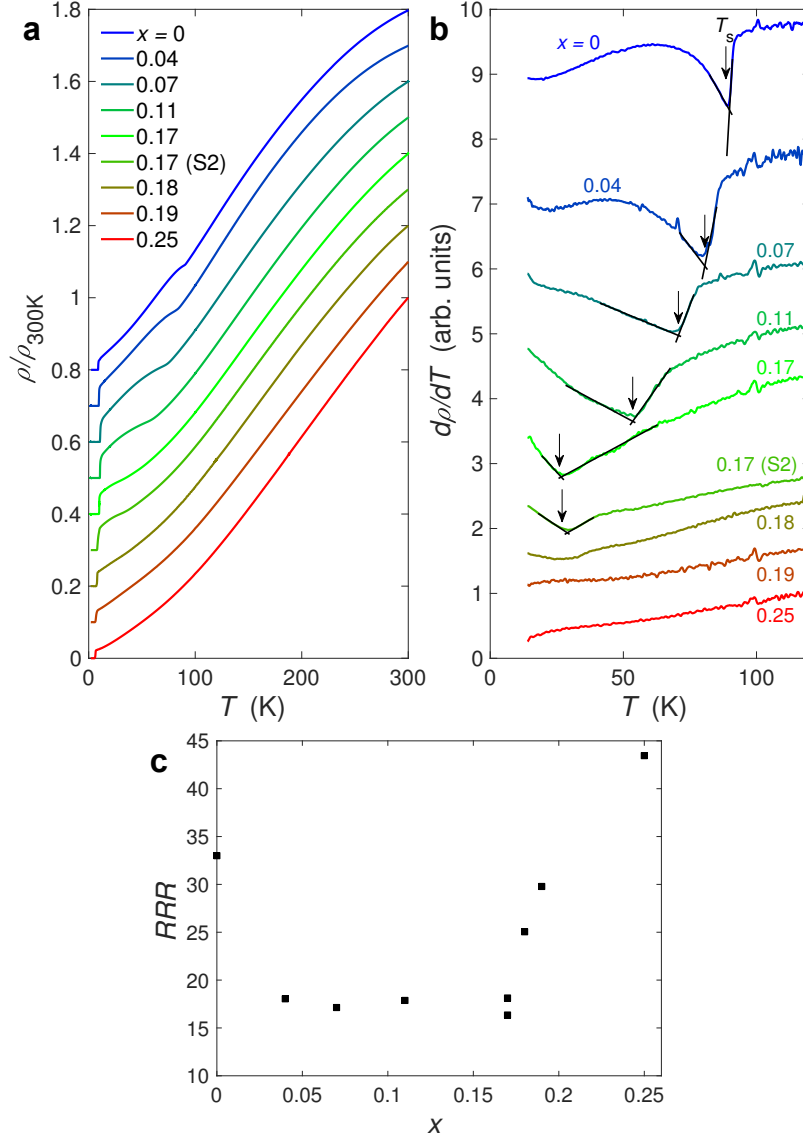


FIG. S1. **Temperature dependence of the resistivity of $\text{FeSe}_{1-x}\text{S}_x$.** (a) Resistivity, normalised to the 300 K value, against temperature for different sulphur concentrations. (b) The first derivative of the resistivity with respect to temperature for the same data. The curves for different sulphur concentrations have been offset for clarity. The location of the structural transition, T_s is defined by the intercept of the linear fits on either side of the transition, as indicated by arrows. (c) The residual resistivity ratio (defined as the ratio between the room temperature and the onset of superconductivity resistivity), RRR , as a function of x . The complete suppression of the structural transition occurs at $x_c \sim 0.180(5)$, which agrees with previous reports [3, 17]. This value however differs from that reported in Ref. [33], where the nominal concentrations have been used. For example, in Ref [33] $x_{\text{nom}} = 0.16$ has $T_s \sim 51$ K, which would correspond to $x \sim 0.13$, based on our phase diagram and previous reports [3, 17]. The two $x \sim 0.17$ and the $x \sim 0.18$ samples come from the same batch and their differences reflect the sulphur variation and the degree of disorder ($x \sim 0.18$ is cleaner with an RRR of ~ 24 compared with ~ 16 for the two $x \sim 0.17$ samples). For $x \sim 0.18$ the derivative in (b) evolves more gradually, without a well-defined structural transition as compared to the others, and we believe that this sample is the closest to the nematic end point (just inside the nematic state).

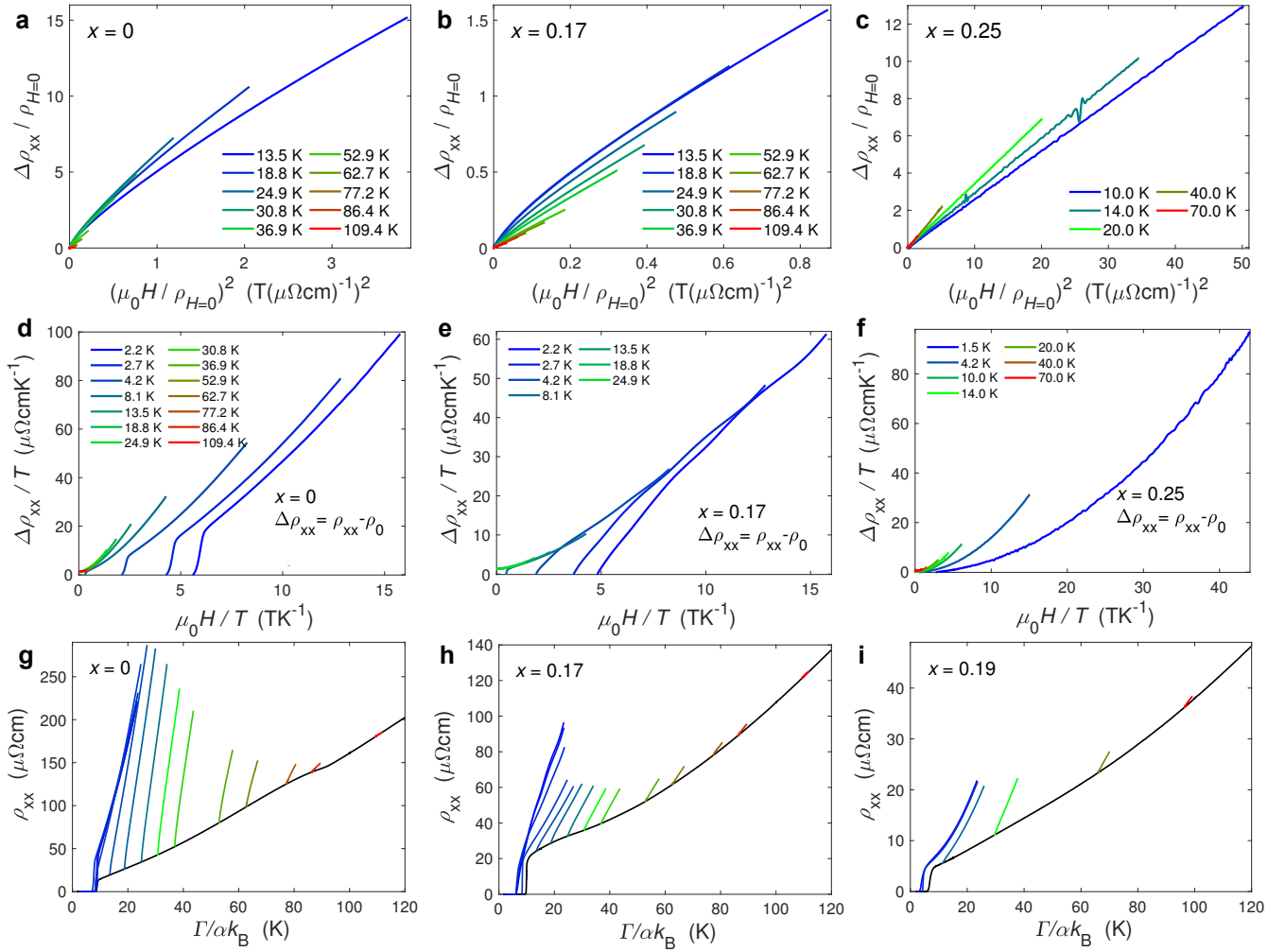


FIG. S2. **The magnetoresistance scaling in $\text{FeSe}_{1-x}\text{S}_x$.** (a-c) Kohler's plots, $\Delta\rho_{xx}(\mu_0 H)/\rho_{xx}(H=0) \sim (\mu_0 H/\rho_{xx}(H=0))^2$, where $\Delta\rho_{xx} = \rho_{xx} - \rho_{xx}(H=0)$ for $x = 0, 0.17$ and 0.25 , respectively. Kohler's rule is clearly violated for all samples over a large temperature range, providing evidence that electrical transport in these systems is not governed by a single scattering time. (d-f) $H - T$ scaling of $\Delta\rho_{xx}/\rho_0 \sim \mu_0 H/T$, where $\Delta\rho_{xx} = \rho_{xx} - \rho_0$ and ρ_0 is the zero-temperature zero-field resistivity. There is clearly no scaling for $x = 0$ and 0.25 ; for the $x = 0.17$ sample in the vicinity of the nematic end point, data are dominated by a low-frequency quantum oscillation and collapse onto a single curve at low temperature, as shown in (e), but we have not identified yet an appropriate scaling law for it. However, in Ref. [30] for a particularly dirty sample of $x_{nom} = 0.18$ with $RRR \sim 5$ and weak magnetoresistance (a factor ~ 100 smaller than our $x \sim 0.17$) H/T scaling was proposed suggesting that disorder may play an important role in this type of scaling in $\text{FeSe}_{1-x}\text{S}_x$. (g-i) Energy scaling of resistivity as Γ , where $\Gamma = \alpha k_B T \sqrt{1 + (\beta/\alpha)^2 (\mu_B \mu_0 H / (k_B T))^2}$ using $\alpha = 1$ and $\beta = 1$, for $x = 0, 0.17$ and 0.19 , respectively. Our data do not follow the proposed energy scaling for any reasonable value of α/β and for any sulphur concentration in $\text{FeSe}_{1-x}\text{S}_x$. This magnetoresistance scaling was used to describe the antiferromagnetic critical region in $\text{BaFe}_2(\text{As}_{1-x}\text{P}_x)_2$ [4].

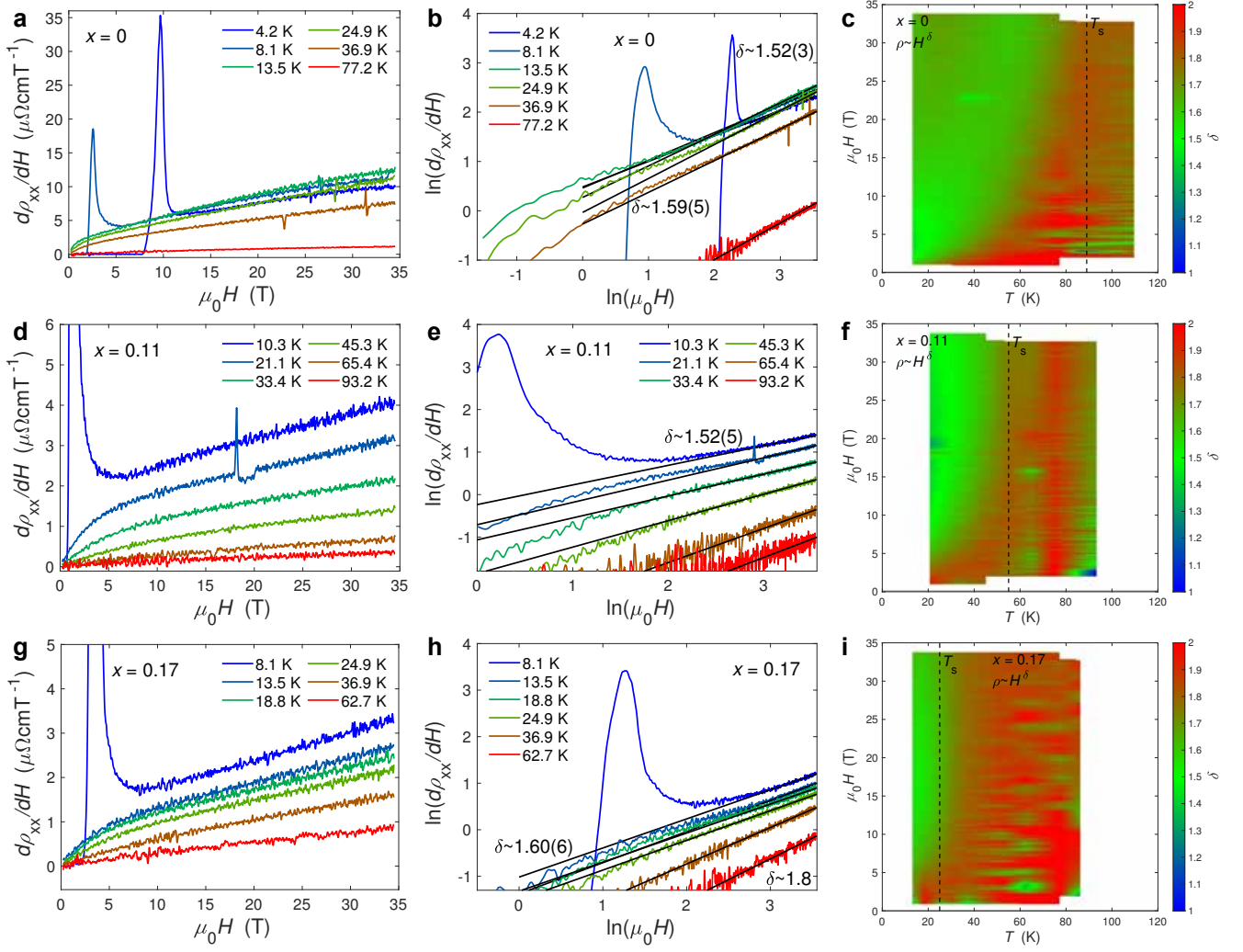


FIG. S3. **Extraction of the magnetic field exponent δ , from the relationship $\rho_{xx} = \rho_{H \rightarrow 0} + bH^\delta$, for $\text{FeSe}_{1-x}\text{S}_x$.** (a, d, g) Derivative of the symmetrized transverse resistivity with respect to the applied magnetic field for $x = 0, 0.11$ and 0.17 , respectively. (b, e, h) Natural logarithm of the derivative against the natural logarithm of magnetic field for the same data in (a, d, g). Here linear fits to the high-field region allow the extraction of the magnetic field exponent from the gradient $\delta - 1$. (c, f, i) Colour plots of δ in the temperature-magnetic field plane, extracted above the superconducting transition temperature using the relationship $d \ln(\rho_{xx} - \rho_{xx}(H=0)) / d(\ln(\mu_0 H)) = \delta$. Consistent values of δ were obtained from linear fits over small regions using $\ln(\rho_{xx} - \rho_{xx}(H=0)) = \ln(b) + \delta \ln(\mu_0 H)$. Our findings clearly show the evolution of the magnetic field exponent from $\delta \sim 1.55(5)$ inside the nematic state towards $\delta \sim 2$ outside of the nematic state.

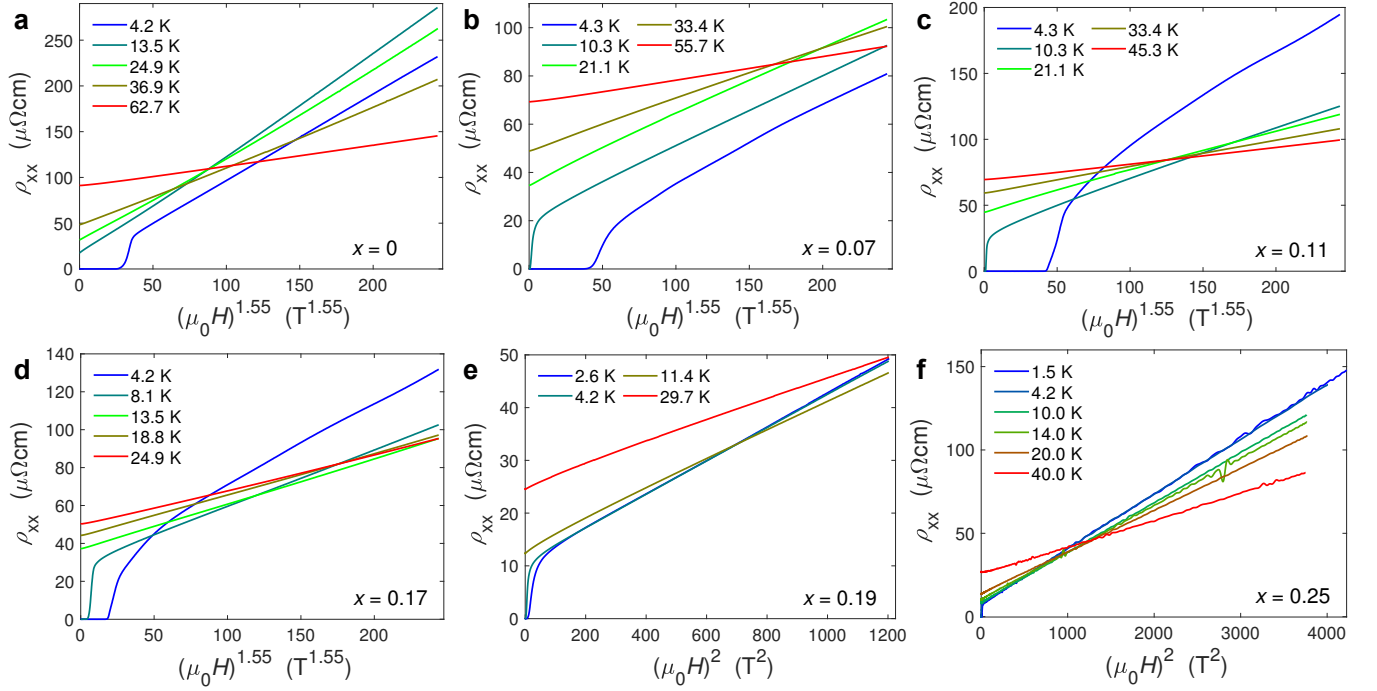


FIG. S4. **Field dependence of the transverse magnetoresistance of $\text{FeSe}_{1-x}\text{S}_x$ over a large magnetic field window.** (a-d) Resistivity as function of $(\mu_0 H)^{1.55}$ showing linear dependence for samples inside the nematic phase at constant temperatures below T_s up to a magnetic field of 35 T. At the lowest temperatures, below ~ 4.2 K, the magnetoresistance is dominated by quantum oscillations. (e-f) Resistivity versus $(\mu_0 H)^2$ at constant temperatures for samples in the tetragonal phase. Data for $x = 0.25$ were measured up to ~ 69 T.

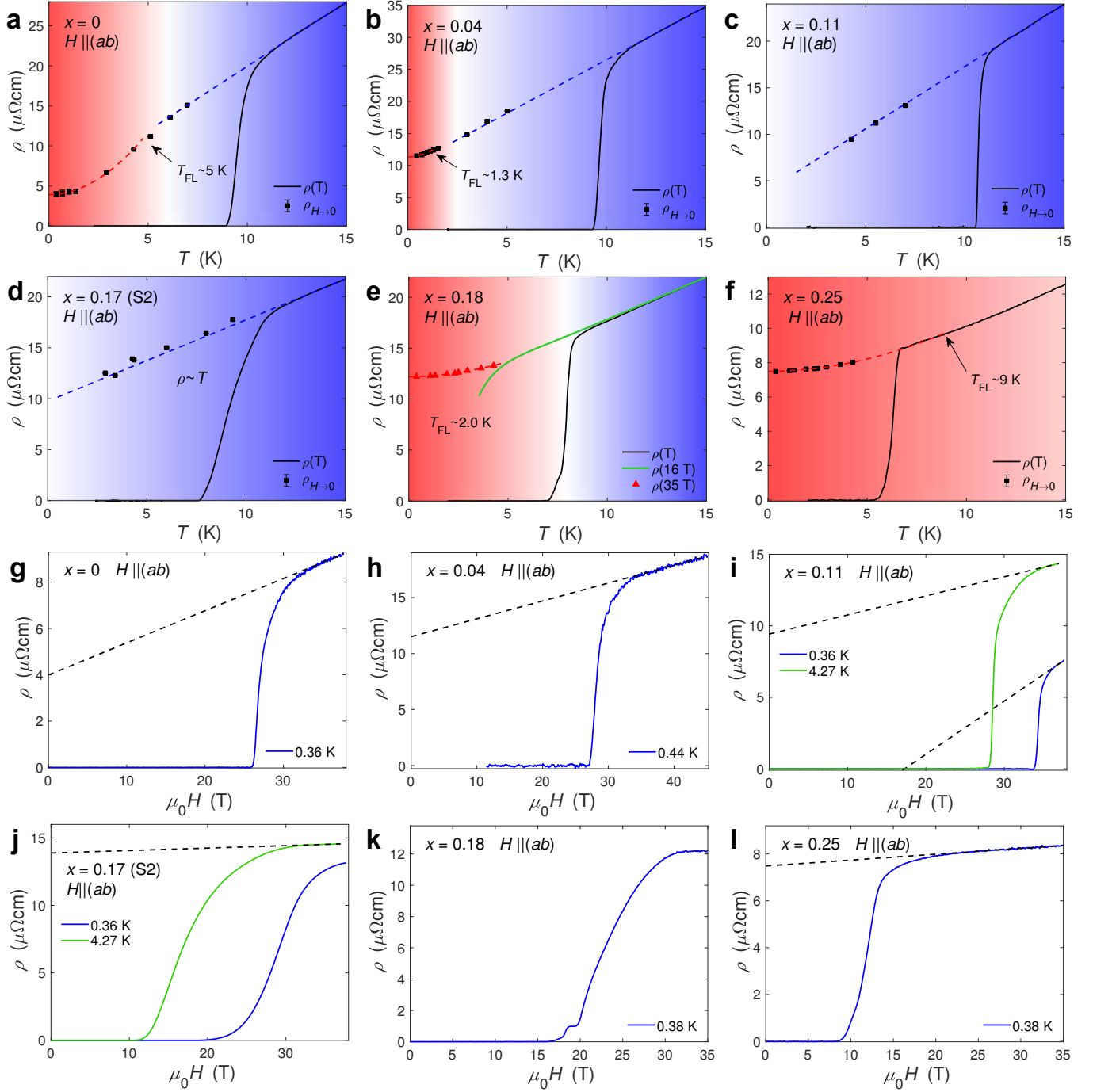


FIG. S5. **The low-temperature resistivity extracted from longitudinal magnetoresistance data of FeSe_{1-x}S_x.** (a-f) Temperature dependence of resistivity at low temperatures for different compositions used to build the low-temperature phase diagram in Fig. 3(b). Solid squares show the extrapolated normal state resistivity, $\rho_{H \rightarrow 0}$ from (g-l), and the solid triangles in (e) are the resistivity data at 35 T from (k), when the magnetic field is along the conducting (ab) plane. Solid lines are the zero-field resistivity for each sample. Fermi-liquid like behaviour is observed in certain samples (with the largest resistivity ratio in Fig.S1(c)) below T_{FL} , as indicated by arrows. (g-l) Magnetic field-dependence of the resistivity at the lowest temperature when $H \parallel (ab)$. Dashed lines are the linear extrapolation towards $H \rightarrow 0$. For $x = 0.11$ and 0.17 , the upper critical field is too large to reach the normal state in magnetic fields up to 38 T in this orientation.

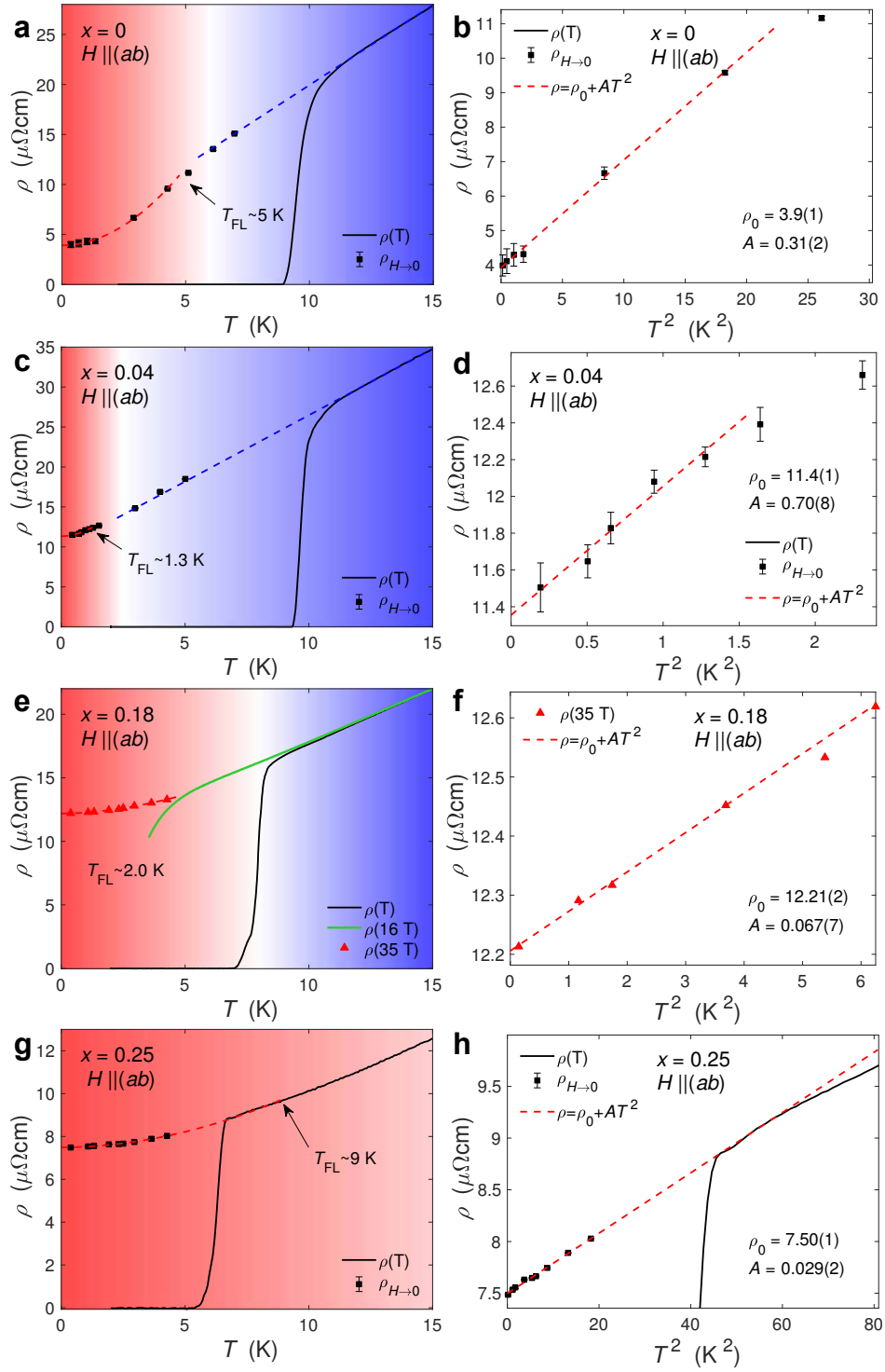


FIG. S6. Evidence of Fermi liquid behaviour in certain samples of $\text{FeSe}_{1-x}\text{S}_x$. (a, c, e, g) Temperature dependence of resistivity at low temperatures for different samples which show Fermi-liquid behaviour, extracted as detailed previously in Fig. S5. The red dashed lines are fits of resistivity to a quadratic temperature dependence below T_{FL} , and the blue dashed lines show a linear dependence between $\sim T_{\text{FL}}$ and T^* . Resistivity data taken at 16 T for $x \sim 0.18$ is also shown in (e) and follows the zero field curve at high temperatures as expected for longitudinal magnetoresistance. (b, d, f, h) The temperature dependence of resistivity against T^2 illustrating the Fermi-liquid behaviour, given by $\rho = \rho_0 + AT^2$. Here the dashed red lines are linear fits in T^2 and the zero-temperature resistivity values, ρ_0 , and A parameters are listed in each panel. We find that the samples with the larger RRR also display larger T_{FL} .

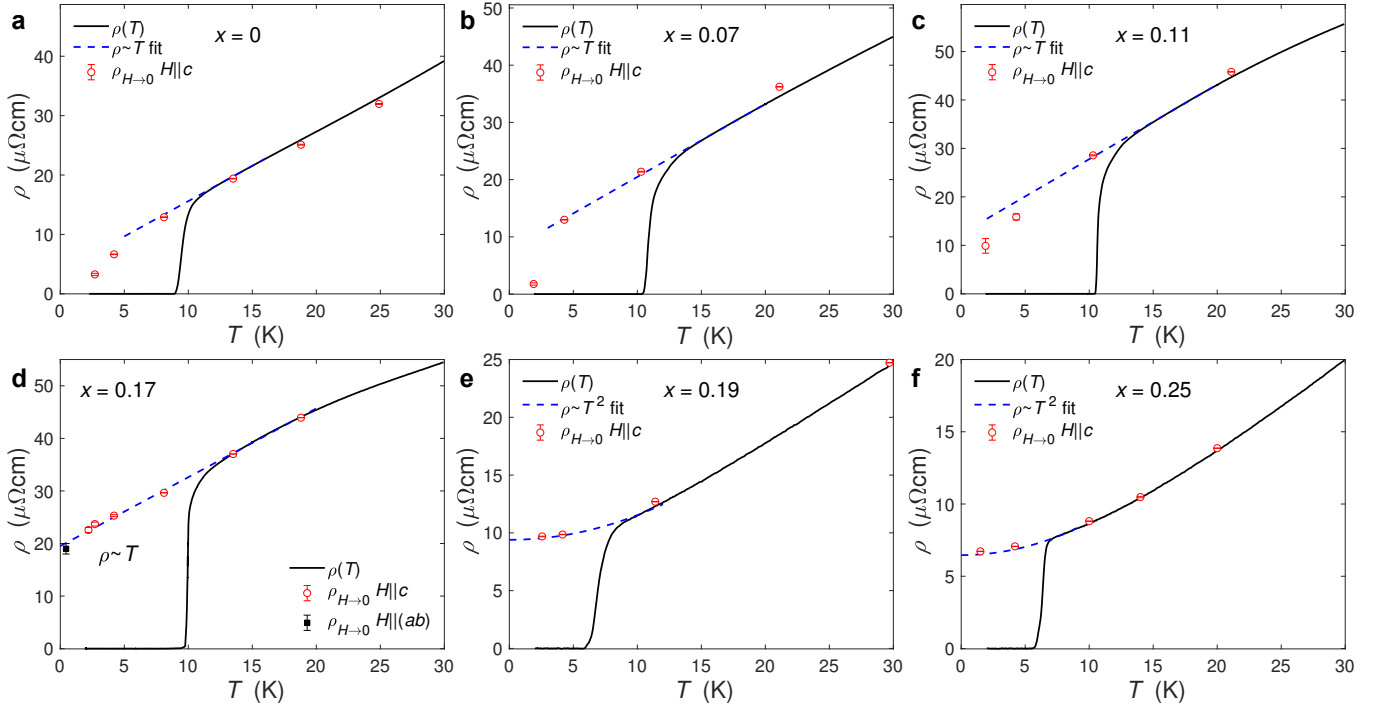


FIG. S7. **The low-temperature transport behaviour based on transverse magnetoresistance for $\text{FeSe}_{1-x}\text{S}_x$.** (a-f) Low temperature resistivity against temperature for different compositions. The open circles in each panel correspond to the extrapolated resistivity (from symmetrized magnetic field data) up to 35 T, using the magnetic field exponents of $\delta = 1.55$ inside the nematic state ($x \lesssim 0.18$) and $\delta = 2$ in the tetragonal state ($x = 0.19 - 0.25$), as shown in Fig. S4. Inside the nematic phase the presence of quantum oscillations at low temperatures, makes the extrapolation of $\rho_{H \rightarrow 0}$ more difficult in this orientation when compared with longitudinal magnetoresistance studies, shown in Fig. S5. In the tetragonal phase, Fermi-liquid behaviour is confirmed, similar to the longitudinal magnetoresistance studies in Fig. S5(f). Dashed lines are either linear fits to the resistivity inside the nematic state or quadratic fits in the tetragonal state. Linear resistivity is found in the vicinity of the nematic end point for $x \sim 0.17$ using both transverse and longitudinal magnetoresistance studies.

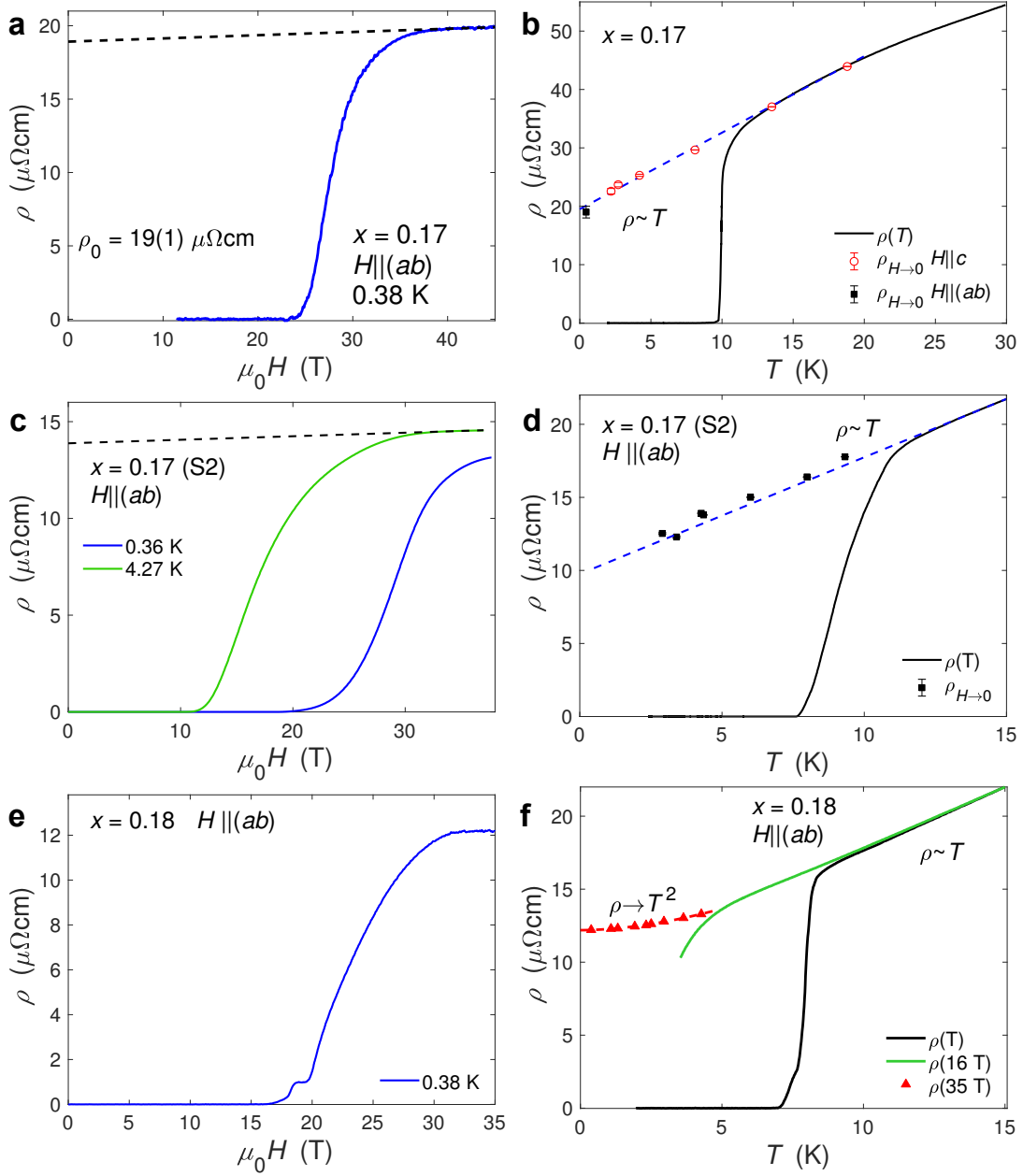


FIG. S8. **The low-temperature transport behaviour in the proximity of the nematic end point in FeSe_{1-x}S_x.** The nematic end point is defined as the complete suppression of the structural transition at $x_c \sim 0.180(5)$, which agrees with previous reports [3, 17]. (a, c, e) Resistivity against magnetic field up to 45 T at the lowest temperatures (~ 0.38 K) for three different samples from the same batch with $H \parallel (ab)$. For sample $x \sim 0.17$ (S2) extracting $\rho_{H \rightarrow 0}$ at the lowest temperatures is not possible up to 38 T and measurements at ~ 4.2 K, are also shown in (c). (b, d, f) Resistivity against temperature for the same samples. Here the solid curves show the zero-field resistivity data and solid black squares are the extrapolated $\rho_{H \rightarrow 0}$ from $H \parallel (ab)$ field sweeps in (a, c). Solid triangles in (f) are the resistivity at 35 T shown in (e). Dashed blue lines in (b) and (d) show a linear dependence, and the red dashed line in (f) show a Fermi-liquid behaviour for $x \sim 0.18$. The sample in which we find Fermi-liquid behaviour has a larger RRR of ~ 24 compared to ~ 16 of the two other samples, suggesting that Fermi-liquid behaviour is observed only in cleaner samples.

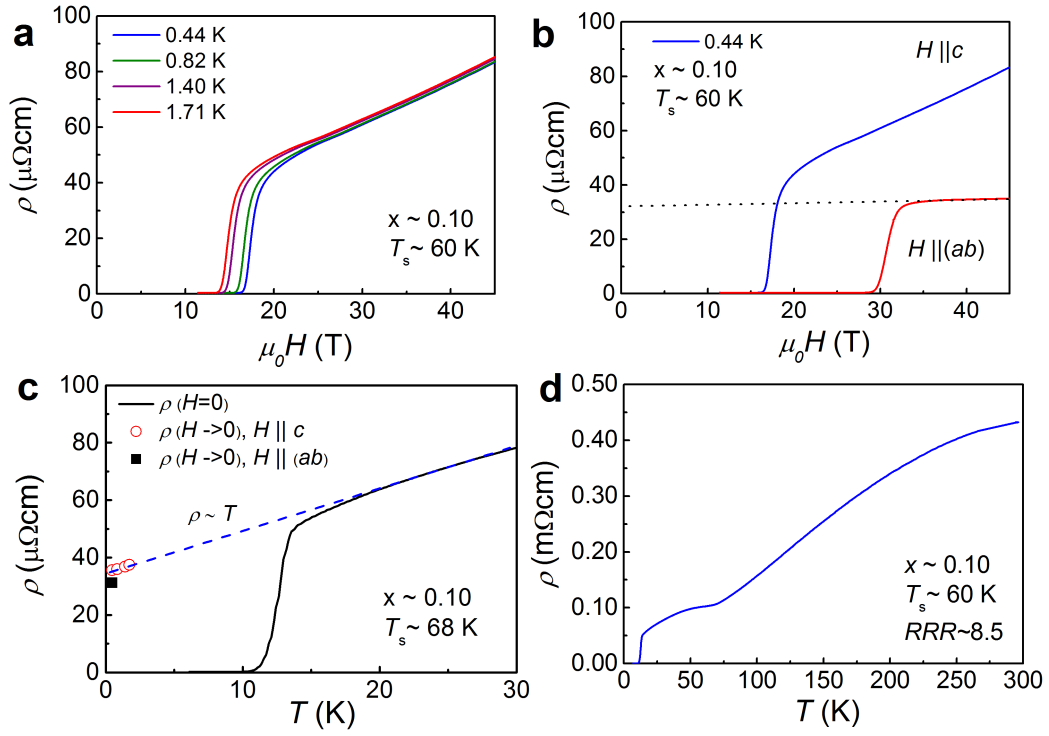


FIG. S9. **Magnetotransport data of a dirtier sample of $\text{FeSe}_{1-x}\text{S}_x$, with $x \sim 0.10$.** (a) Resistivity as a function of magnetic field at constant low temperatures with $H \parallel c$. (b) Resistivity against magnetic field for two different orientations at base temperature, $H \parallel c$ and $H \parallel (ab)$. (c) Zero-resistivity data (solid curve) together with zero-field extrapolation using both linear extrapolation for $H \parallel (ab)$ (solid square) from (b) and zero-field extrapolation using a $H^{1.55}$ dependence for $H \parallel c$ (open circles) from (a). (d) Resistivity versus temperature for $x \sim 0.10$ with $RRR \sim 8.5$. The strong suppression of quantum oscillations and the low RRR in this sample are evidence that it is a dirtier system which also display linear resistivity down to the lowest temperatures measured (~ 0.44 K).

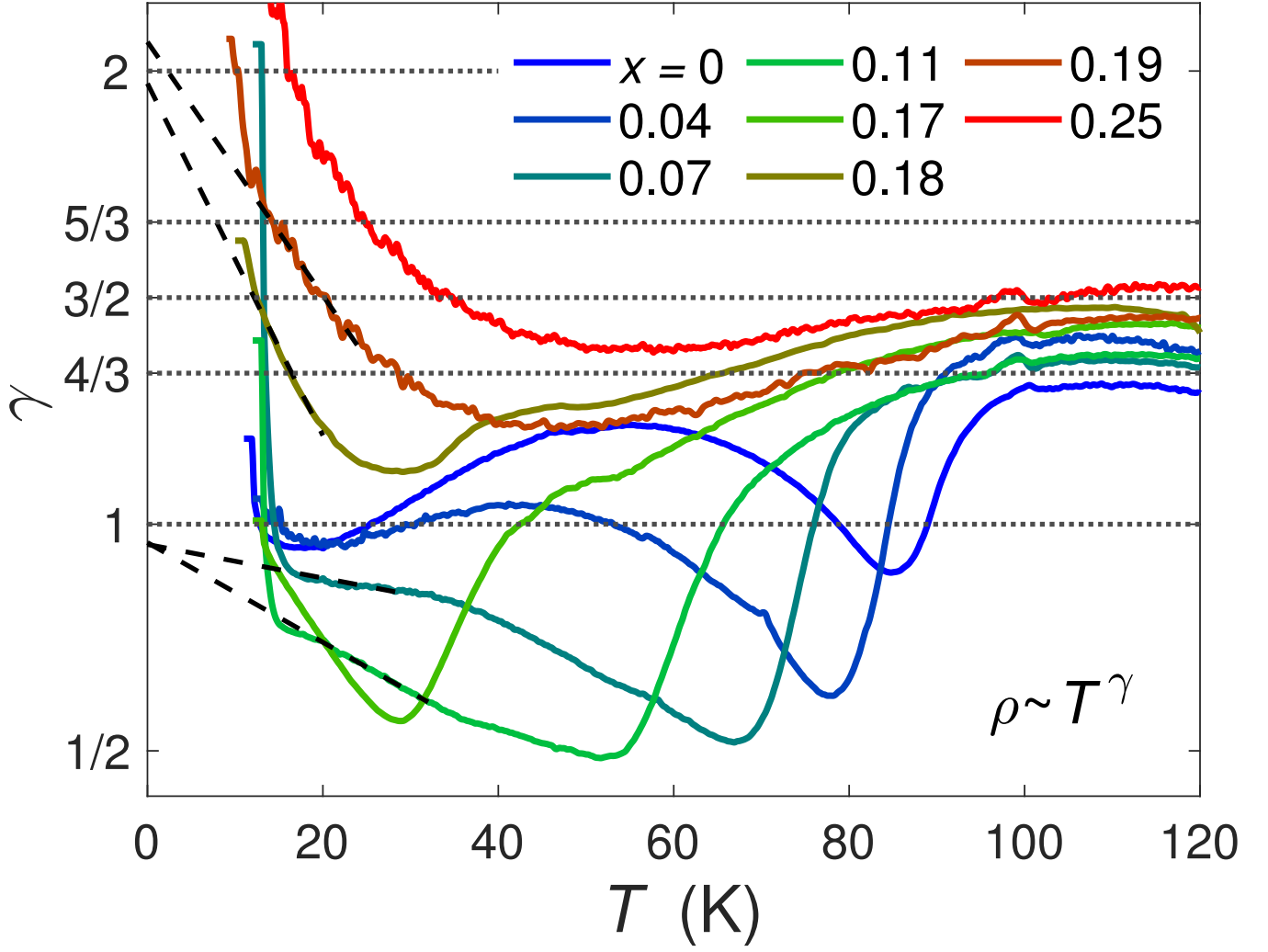


FIG. S10. **The temperature dependence of the exponent γ from $\rho = \rho_0 + AT^\gamma$ for $\text{FeSe}_{1-x}\text{S}_x$.** The γ exponent is estimated a $\gamma = d\ln(\rho - \rho_0)/d\ln(T)$ for various sulphur concentrations. The ρ_0 values are the zero-field zero-temperature resistivity extracted from Figs. S5, S6 and S7. The curves shown here were used to generate the colour plots in Fig. 3(a) and (b) in the main body of the paper. Dashed black lines show possible extrapolations of the exponent towards the zero temperature limit. The horizontal lines indicated different possible exponents predicted by theory in the vicinity of a critical point [31, 35, 40]. The γ exponent depends on the value of ρ_0 , which was extracted at the lowest temperature from longitudinal magnetoresistance in Fig. S5.

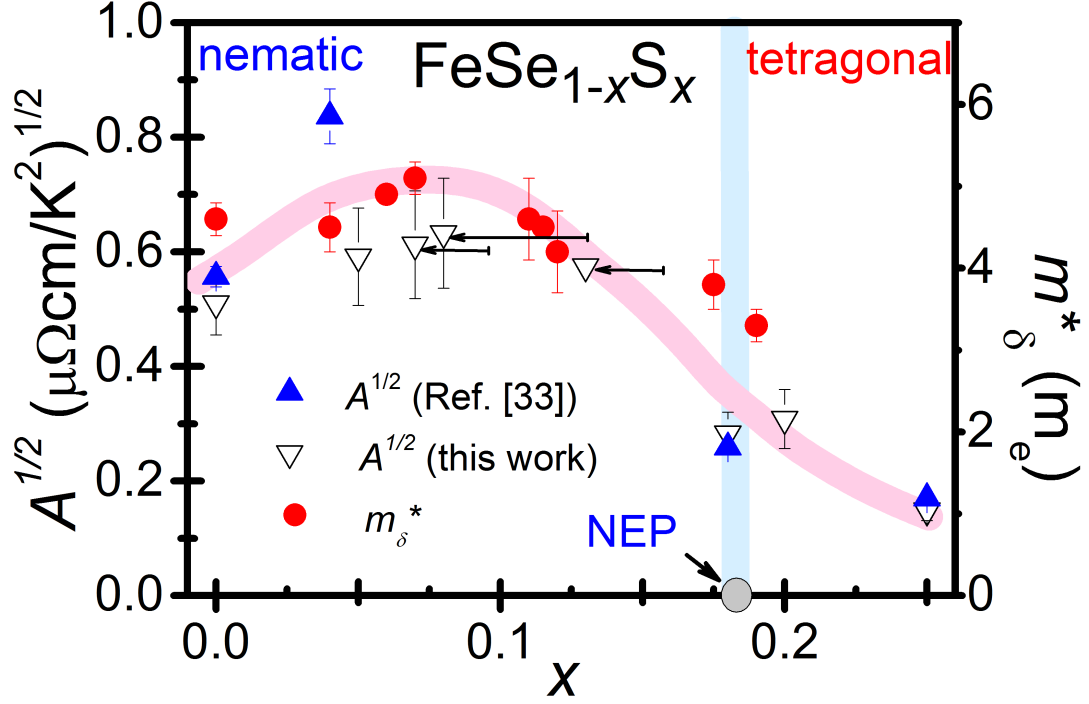


FIG. S11. Comparison between the $A^{1/2}$ temperature coefficient and the effective masses for different compositions of $\text{FeSe}_{1-x}\text{S}_x$. The band masses of the δ orbit (from Ref. [3]) are compared to the Fermi liquid coefficient, A , extracted at low temperatures (solid triangles) for compositions that show Fermi-liquid behaviour, as shown in Fig.S6. Data reported in Ref.[33] are also included for comparison as open triangles. Please note that Ref.[33] uses nominal x_{nom} values which are shifted to smaller values (as indicated by horizontal arrows) to match the real x values based on EDX studies reported previously [3, 17]. The nematic end point (NEP) is indicated by an arrow and circle around $x \sim 0.180(5)$. Solid thick lines are guides to the eye.